Mathematical modeling reveals the functional implications of the different nuclear shuttling rates of Erk1 and Erk2

2012 Phys. Biol. 9 036001

(http://iopscience.iop.org/1478-3975/9/3/036001)

Phys. Biol. **9** (2012) 036001 (12pp) doi:10.1088/1478-3975/9/3/036001

Mathematical modeling reveals the functional implications of the different nuclear shuttling rates of Erk1 and Erk2

Heather A Harrington[1], **Michał Komorowski**[1], **Mariano Beguerisse-Díaz**[2], **Gian Michele Ratto**[3] **and Michael P H Stumpf**[1,4]

[1] Division of Molecular Biosciences, Imperial College London, London, UK
[2] Division of Biology and Department of Mathematics, Imperial College London, London, UK
[3] Istituto Nanoscienze and Scuola Normale Superiore, Pisa, Italy

E-mail: m.stumpf@imperial.ac.uk

Received 28 November 2011
Accepted for publication 12 March 2012
Published 3 May 2012
Online at stacks.iop.org/PhysBio/9/036001

Abstract
The mitogen-activated protein kinase (MAPK) family of proteins is involved in regulating cellular fates such as proliferation, differentiation and apoptosis. In particular, the dynamics of the Erk/Mek system, which has become the canonical example for MAPK signaling systems, have attracted considerable attention. Erk is encoded by two genes, Erk1 and Erk2, that until recently had been considered equivalent as they differ only subtly at the sequence level. However, these proteins exhibit radically different trafficking between cytoplasm and nucleus and this fact may have functional implications. Here we use spatially resolved data on Erk1/2 to develop and analyze spatio-temporal models of these cascades, and we discuss how sensitivity analysis can be used to discriminate between mechanisms. Our models elucidate some of the factors governing the interplay between signaling processes and the Erk1/2 localization in different cellular compartments, including competition between Erk1 and Erk2. Our approach is applicable to a wide range of signaling systems, such as activation cascades, where translocation of molecules occurs. Our study provides a first model of Erk1 and Erk2 activation and their nuclear shuttling dynamics, revealing a role in the regulation of the efficiency of nuclear signaling.

S Online supplementary data available from stacks.iop.org/PhysBio/9/036001/mmedia

Introduction

Cellular decision-making processes require balanced and nuanced responses to environmental, physiological and developmental signals. In particular, in eukaryotes this involves the interplay and concerted action of a number of molecular players, which receive external signals, broadcast them further into the cytoplasm and, if a transcriptional response is called for, shuttle into the nucleus and activate the transcriptional machinery. The mitogen-activated protein kinases (MAPK) are important relays in many of these signal transduction processes. They are, for example, involved in regulating cellular fates such as proliferation, differentiation and apoptosis [1]. The most widely studied MAPK, Erk, is activated through phosphorylation by Mek, its MAPK kinase (MAPKK), and Mek in turn is activated by its cognate kinase. Activated kinases, such as Erk or Mek, are deactivated via dephosphorylation by their respective phosphatases.

The cellular localization of Erk depends on the regulated equilibrium between cytoplasmic and nuclear anchors [2–4]

[4] Author to whom any correspondence should be addressed.

and on the diffusion/transport through the nuclear membrane. Movement through the nucleoporin proceeds through a variety of mechanisms, both energy independent and energy dependent [5, 6], particularly through the mediation by importin 7 [7–9]).

Regardless of the nature of Erk transport through the nuclear pore, the final action of Erk on its nuclear targets depends on how cytoplasmic activation of these kinases is transmitted into the nucleus. It has been shown that Erk continuously shuttles between the nucleus and cytoplasm [10–14]: since the activation of Erk occurs mainly in the cytoplasm, while dephosphorylation is prevalent in the nucleus [15], the continuous influx of phosphorylated Erk is necessary to support Erk activity, such as transcriptional control, in the nucleus. But Erk is encoded by two genes, Erk1 and Erk2, and recently it was found that Erk1 shuttles at a lower rate than Erk2 [16]: this suggests that Erk1 might be less able than Erk2 to maintain its activation state upon translocation.

Erk1 and Erk2 appear to have distinctly different biological characteristics. For example, transgenic gene knockout mice lacking Erk2 ($Erk2^{-/-}$) result in embryonic lethality, whereas $Erk1^{-/-}$ are viable, fecund and suffer from only subtle deficiencies, e.g., reduced T cell development [17, 18]. This might be due to the different expression levels of the two proteins (Erk2 is much more abundant than Erk1) [19] but there might be other factors contributing to different catalytic efficiencies of Erk1 and Erk2. Recently, it has been demonstrated that the shuttling of Erk1 from the cytoplasm to nucleus is approximately three times slower than that of Erk2, regardless of whether the cell is starved or stimulated [13, 16]; the different rates of shuttling result from differences in the N-terminal domain of Erk1 and Erk2 [14].

Activation cascades have been studied extensively, but given that experimental results often rely on incomplete or indirect observations of the underlying dynamics, and in light of sometimes partially contradictory experimental results, mathematical models have become increasingly important for understanding these cascades. Published models of activation cascades typically use a feedback structure that can confer ultrasensitivity, bistability and oscillations (with different possible mechanisms and parameter constraints for the various types of behavior) [20–32]. Other authors have explored the cascade in a linear manner in order to study the effects of cascade length, signal transduction efficiency and other facets, in the presence of specific feedback structures [33–35]. Models have also been developed to study the differences between Erk1 and Erk2 [16, 31, 36]. A tiered model with Erk1, Erk2, Mek and upstream species of the cascade has also been developed, identifying that Erk isoforms cross-regulate each other in a way that affects cell fate decisions [36]. The role in the activation/deactivation activity of Erk in both the nucleus and cytoplasm has motivated the recent development of spatio-temporal models [31, 37–40]. A compartment model of MAPK using single feedback loops [37] was extended to include double phosphorylation/dephosphorylation loops [38]. Another model focused on Erk1 dimerization using data from Erk1 wild type and the Erk1-Δ4 mutant (unable to dimerize) and improved an earlier nuclear transport model [37] by exploring different methods of phosphorylation [31]. Finally, a simple model including only Erk1 and Erk2 species was constructed to study the nucleo-cytoplasmic shuttling speeds [16].

The existence of two genetically nearly identical Erk proteins is difficult to explain, especially in light of the above observation. Here we seek to understand potential dynamical reasons for the existence of the Erk1 and Erk2. To do so we have to consider their interactions with Mek and nuclear/cytoplasmic shuttling. We integrate these different processes into a single model and compare it to recent spatio-temporally resolved data, and consider and contrast the behavior in two cell types, HeLa and NIH 3T3, and under different conditions. We find that shuttling, a hitherto ignored spatial aspect, exerts great influence on the capacity of Erk to phosphorylated nuclear targets and this contributes to differences in the actions of Erk1 and Erk2. Our model supports the biological relevance of the recently posed hypothesis [41] of the importance of competition between Erk1 and Erk2.

In this study, we have developed a model of Erk activation that includes explicitly the shuttling process through the nuclear membrane; this will allow us to investigate the importance of the Erk1 and Erk2 shuttling rates for determining nuclear signaling dynamics.

Materials and methods

A spatio-temporal model of Erk signaling

A reaction network of the spatio-temporal model is built around Erk1, Erk2 and Mek, which are allowed to exist in different activation states, as complexes and in different cellular compartments (see figure 1(*a*) and find equations in supplementary material available at stacks.iop.org/PhysBio/9/036001/mmedia). We assume that Erk exists in one of three states: inactive (Erk), bound to Mek (M-Erk) or active (Erk*p*). Upon Mek–Erk binding and forming of an intermediary complex (M-Erk), Mek phosphorylates Erk resulting in activated Erk (Erk*p*) and then dissociates from Erk*p*. In order for Erk*p* to revert back to its inactive form, it must undergo dephosphorylation by a phosphatase. To denote the subcellular compartment of Erk, species are denoted by a subscript, n, to indicate nuclear localization, i.e. $Erk1_n$ is Erk1 in the nuclear compartment. The biochemical reactions of the full system are given in table 1 with a description in table 3. Shuttling rates of Erk in HeLa cells have previously been established; however, to determine the shuttling of Erk species in NIH 3T3 cells, we used FRAP analysis, as shown in figure 2, and these data enabled us to estimate transport rates.

Cell culture and transfection

NIH 3T3 cells were plated on glass disks cultured in modified Dulbecco's medium supplemented with 10% fetal bovine serum and were transfected using Lipofectamine (GenePORTER 2, Genlantis, San Diego, CA). To inactivate

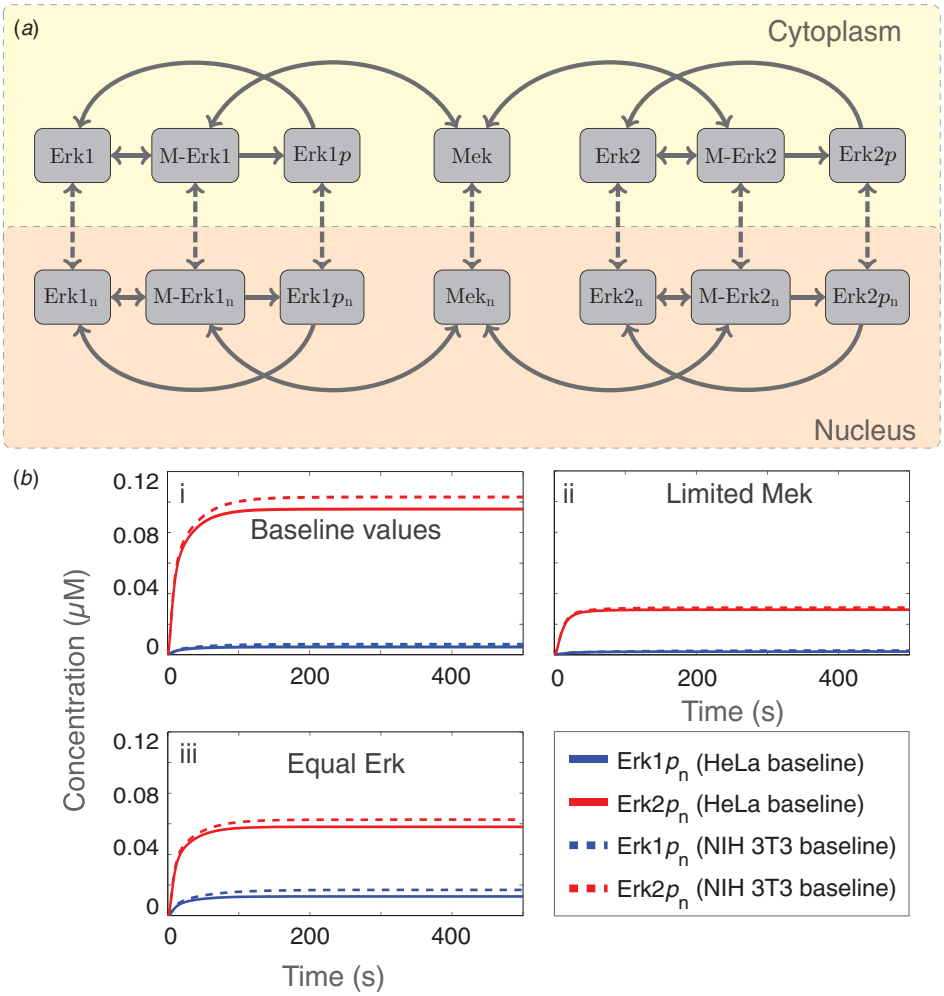

Figure 1. (*a*) Schematic of the full Erk/Mek shuttling model. Reactions (solid arrows) can occur in either the cytoplasm (yellow region) or nucleus (orange region) and all model species (gray boxes) can shuttle between compartments (dashed arrows). (*b*) Time course of nuclear Erk1p_n and Erk2p_n that reaches steady state for HeLa and NIH 3T3 cells. (i) Time course at baseline conditions. (ii) Time course at limited Mek (Mek(0) = 0.2). (iii) Time course at equal Erk1/2 (Erk1(0) = Erk2(0) = 0.5).

Table 1. Reactions of Erk1/2 and Mek in the full model. Each reaction highlights whether it is a forward or reversible reaction by the arrows as illustrated by the solid arrows in figure 1(*a*). All reaction rates are from [37].

Number	Reaction	Forward rate (μM^{-1} s^{-1})	Reverse rate (s^{-1})
1	Erk1 + Mek ⇌ M-Erk1	8.8×10^{-1}	8.8×10^{-2}
2	M-Erk1 → Mek + Erk1p	3×10^{-1}	
3	Erk1$_n$ + Mek$_n$ ⇌ M-Erk1$_n$	8.8×10^{-1}	8.8×10^{-2}
4	M-Erk1$_n$ → Mek$_n$ + Erk1p_n	3×10^{-1}	
5	Erk2 + Mek ⇌ M-Erk2	8.8×10^{-1}	8.8×10^{-2}
6	M-Erk2 → Mek + Erk2p	2×10^{-1}	
7	Erk2$_n$ + Mek$_n$ ⇌ M-Erk2$_n$	8.8×10^{-1}	8.8×10^{-2}
8	M-Erk2$_n$ → Mek$_n$ + Erk2p_n	2×10^{-1}	
9	Erk1p → Erk1	1.4×10^{-2}	
10	Erk1p_n → Erk1$_n$	1.4×10^{-2}	
11	Erk2p → Erk2	1.4×10^{-2}	
12	Erk2p_n → Erk2$_n$	1.4×10^{-2}	

the Erk pathway, cells were starved by keeping them in 1% FBS for 24 h before imaging. Further details and the design of the Erk-GFP fusion proteins are found in [13, 16]. Expression levels of Erk1 and 2 were kept to a minimum (under 150 nm) in order not to perturb the stoichiometry between Erk and Mek (see [13] for details).

FRAP measure of nucleus–cytoplasm shuttling

Photo bleaching was preceded by the acquisition of a pre-bleach image that was used to estimate the loss of fluorescence due to bleaching and for data normalization. The nucleus of the cell was photobleached by repeated scans of the nucleus at high laser power. Bleaching was applied for approximately 8 s, which was sufficient to quench most of the nuclear fluorescence. Bleaching was followed by time-lapse acquisition to measure the recovery. Fluorescence was normalized by

$$F(t) = \frac{F_{\mathrm{Tot}}}{F_{\mathrm{Nuc}}} \cdot \frac{F_{\mathrm{Nuc}}(f)}{F_{\mathrm{Tot}}(t)},$$

where F_{Tot} indicates the fluorescence (corrected for background) measured before bleaching in the entire cell and F_{Nuc} indicates the same measure in the nucleus. This normalization corrects for bleaching caused by imaging. All

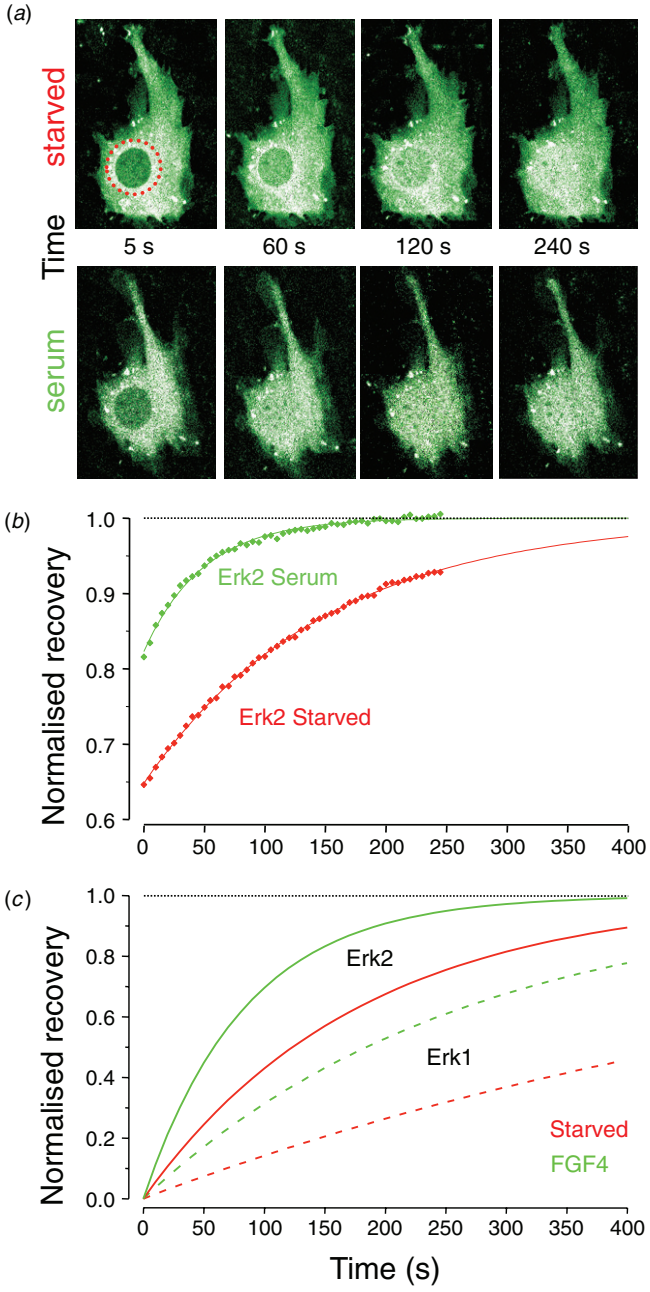

Figure 2. (*a*) Imaging of NIH 3T3 fibroblasts transfected with Erk2-GFP. Trafficking rates have been measured by analyzing the speed of recovery of fluorescence after bleaching of the nucleus (red dots in the first image). Nuclear fluorescence is bleached at time 0 and the time lapse sequence shows its recovery. After complete recovery, the cells are stimulated with 10% serum and, after allowing 15 min for maximal Erk activation, a second bleach-recovery sequence is acquired. The calibration bar is 10 μm. (*b*) Time course of the fluorescence recovery acquired for the illustrated cell before (red) and after activation of the Erk pathway (green). The continuous lines represent fitting exponentials of time constants 152 and 49 s, respectively. (*c*) Erk1 and Erk2 have different trafficking rates: the four exponentials indicate the normalized time course of the fluorescence recovery for Erk1 (dotted lines) and Erk2 (continuous lines) in the starved condition (red) and after stimulation (green). Rates have been obtained from averaging rates measured in 30–60 cells in each condition (5).

imaging experiments were performed on Olympus Fluoview 300 and Leica SL confocal microscopes.

Model parameterization

We focus our analysis on HeLA cells and mouse NIH 3T3 cells. Phosphorylation, shuttling rates and initial conditions have previously been specified for HeLa cells [37, 42], whereas shuttling rates here have been measured in mouse NIH 3T3 cells [13, 16]. We use the kinetic phosphorylation and dephosphorylation parameters for an initial estimate for Erk2 from the compartment model of Erk2 in HeLa cells using a single phosphorylation loop [37]. Erk1 is phosphorylated slightly faster than Erk2 in primary erytheroid progenitor (CFU-E) cells [36] and we adjust the baseline parameter (k_2) value for the complete model to take this into account (table 1).

Both HeLa and NIH 3T3 cells are 15–20 μm in diameter and have approximately the same volume. The import and export shuttling rates between the cytoplasm and nucleus include the ratio of cytoplasmic to nuclear volume as used in other compartment models [31, 37, 38]. We use the Erk2 shuttling rates in HeLa cells from [37] and then calibrate the shuttling rates to satisfy that Erk1 shuttling is three times slower than Erk2 as seen in figure 2 and [16]. To estimate the transport parameters from the data, the shuttling time constants (τ) were calculated by first photobleaching the nucleus and then measuring the recovery of fluorescence of Erk in NIH 3T3 cells (see [13, 16] for more details). We assume that in starved cells, there is minimal phosphorylation by Mek and primarily inactive Erk shuttles; stimulated cells, on the other hand, shuttle predominantly phosphorylated (Erk*p*) species (supplementary material available at stacks.iop.org/PhysBio/9/036001/mmedia). Transport reactions and shuttling rates can be found in table 2 and a description in table 3.

The non-zero baseline initial concentrations are the cytoplasmic species Erk1, Erk2 and Mek. Estimates of initial levels of Erk in previous MAPK models of HeLa cells ranged between 0.96 and 2.1 μM [37, 42] and most previous models have initial Mek and Erk concentrations varying between 0.1 and 3 μM [37]. In HeLa cells, the ratio of Mek to Erk at the initial conditions is approximately 1.46 [37, 42]. Since we do not include inactive Mek in this model, we estimate that active (phosphorylated) Mek $\approx$ 1 and that the ratio of active (phosphorylated) Mek to Erk is 1. Since Erk in previous models had been assumed to be approximately 1 μM [37, 42], we assume the relation total (phosphorylated)Mek $\approx$ total Erk1 + total Erk2, and the baseline initial concentrations of Erk also satisfy the condition that Erk1 is four times less abundant than Erk2 in NIH 3T3 cells [19]. We also take into account that HeLa cells may have a different ratio of Erk1 and Erk2 or different concentrations of active Mek, either due to initial activation of the MAPK cascade or Mek sequestration effects, etc (table 4).

Steady-state analysis

We investigate the behavior of the system for the baseline parameters and find that only one permissible and biologically

Table 2. Shuttling rates for HeLa and NIH 3T3 cells (shown as dotted arrows in figure 1(*a*)). Parameters are estimated from [37] and * denotes rates from [16].

		Baseline HeLa cells		Baseline NIH 3T3 cells	
Number	Transport	Export Rate (s^{-1})	Import Rate (s^{-1})	Export Rate (s^{-1})	Import Rate (s^{-1})
1	$Erk1 \rightleftharpoons Erk1_n$	1.3×10^{-2}	4×10^{-3} *	2.1×10^{-3} *	1.4×10^{-3} *
2	$Mek \rightleftharpoons Mek_n$	5.4×10^{-1}	4×10^{-2}	5.4×10^{-1}	4×10^{-2}
3	$M\text{-}Erk1 \rightleftharpoons M\text{-}Erk1_n$	2.6×10^{-1}	1.17×10^{-2} *	2.6×10^{-1}	1.17×10^{-2} *
4	$Erk1p \rightleftharpoons Erk1p_n$	1.3×10^{-2}	4×10^{-3} *	5.2×10^{-3} *	4.7×10^{-3} *
5	$Erk2 \rightleftharpoons Erk2_n$	1.8×10^{-2}	1.2×10^{-2}	7.8×10^{-3} *	5.2×10^{-3} *
6	$M\text{-}Erk2 \rightleftharpoons M\text{-}Erk2_n$	2.6×10^{-1}	3.5×10^{-2}	2.6×10^{-1}	3.5×10^{-2}
7	$Erk2p \rightleftharpoons Erk2_n$	1.3×10^{-2}	1.1×10^{-2}	1.65×10^{-2} *	1.5×10^{-2} *

Table 3. Description of model parameters.

Parameters	Description
k_1	Forward interaction rate between cytoplasmic Mek and Erk1
k_{-1}	Reverse interaction rate between cytoplasmic Mek and Erk1
k_2	Phosphorylation rate of cytoplasmic Erk1
k_3	Forward interaction rate between nuclear Mek and Erk1
k_{-3}	Reverse interaction rate between nuclear Mek and Erk1
k_4	Phosphorylation rate of nuclear Erk1
k_5	Forward interaction rate between cytoplasmic Mek and Erk2
k_{-5}	Reverse interaction rate between cytoplasmic Mek and Erk2
k_6	Phosphorylation rate of cytoplasmic Erk2
k_7	Forward interaction rate between cytoplasmic Mek and Erk2
k_{-7}	Reverse interaction rate between cytoplasmic Mek and Erk2
k_8	Phosphorylation rate of nuclear Erk2
k_9	Dephosphorylation rate of cytoplasmic Erk1p
k_{10}	Dephosphorylation rate of nuclear Erk1p
k_{11}	Dephosphorylation rate of cytoplasmic Erk2p
k_{12}	Dephosphorylation rate of nuclear Erk2p
s_1	Import of Erk1 into the nucleus
s_{-1}	Export of Erk1 out of the nucleus
s_2	Import of Mek into the nucleus
s_2	Export of Mek out the nucleus
s_3	Import of M-Erk1 into the nucleus
s_{-3}	Export of M-Erk1 into the nucleus
s_4	Import of Erk1p into the nucleus
s_4	Export of Erk1p out of the nucleus
s_5	Import of Erk2 into the nucleus
s_{-5}	Export of Erk2 out of the nucleus
s_6	Import of M-Erk2 into the nucleus
s_{-6}	Export of M-Erk2 out of the nucleus
s_7	Import of Erk2p into the nucleus
s_{-7}	Export of Erk2p out of the nucleus

relevant steady state exists. Further exploration of the biophysically plausible parameter space of the models using latin-hypercube sampling [43] confirms that there is indeed only one biologically permissible steady state. This finding of the minimal model is in line with previous studies that looked into the classification of single and double phosphorylation cycle networks in terms of whether they yield multistability [44].

Table 4. Initial conditions of the model variables for different cell types. Some species initial conditions may differ due to cell variability or cell type. Baseline values estimated from [16, 37].

	Initial concentration (μM)		
Species	Baseline	Equal Erk 1/2	Limited Mek
Erk1	0.2	0.5	0.2
Erk2	0.8	0.5	0.8
Mek	1	1	0.2

Sensitivity analysis

To study the effects of the parameter values on the dynamics of $Erk1p_n$ and $Erk2p_n$, we performed a detailed and comprehensive sensitivity analysis. We used a method based on the Fisher information [45], which assesses the change in system output as parameters are varied. Suppose that we are interested in the values $Erk1p_n(t)$ and $Erk2p_n(t)$, denoting concentrations of nuclear Erk1p and Erk2p, respectively, at times $t_1, \ldots, t_N$. Then the sensitivity coefficient for a parameter k_i is

$$S_{k_j} = \sum_{j=1}^{N} \left(\frac{\partial Erk1p_n(t_j)}{\partial k_i} \right)^2 + \left(\frac{\partial Erk2p_n(t_j)}{\partial t_j} \right)^2. \quad (1)$$

As the trajectories $x.(t)$ are given by solutions of ordinary differential equations, their derivatives $\partial x.(t)/\partial k_i$ can be easily calculated [46]. We have used this type of sensitivity coefficient as it has a clear information geometric interpretation as the infinitesimal distance in the state space behaves locally as the Kullback–Leibler divergence [47], and allows us to determine directions of trajectory change resulting from parameter changes. Treating the initial conditions as parameters provides us with their sensitivities in an equally simple way [45].

Results

It is well known that the Erk overexpression causes its ectopic nuclear localization due to saturation of the cytoplasmic anchors [3, 48, 49] and docking domain interactions [50, 51]. This could perturb the trafficking properties of Erk and, in principle, could affect the rate constants of the nuclear–cytoplasmic trafficking. Hence, it is relevant to point out that the trafficking data we used have been obtained in a regime of very low overexpression of Erk1 and Erk2 (below 150 nM [13]). In this range, Erk-GFP correctly accumulates in the

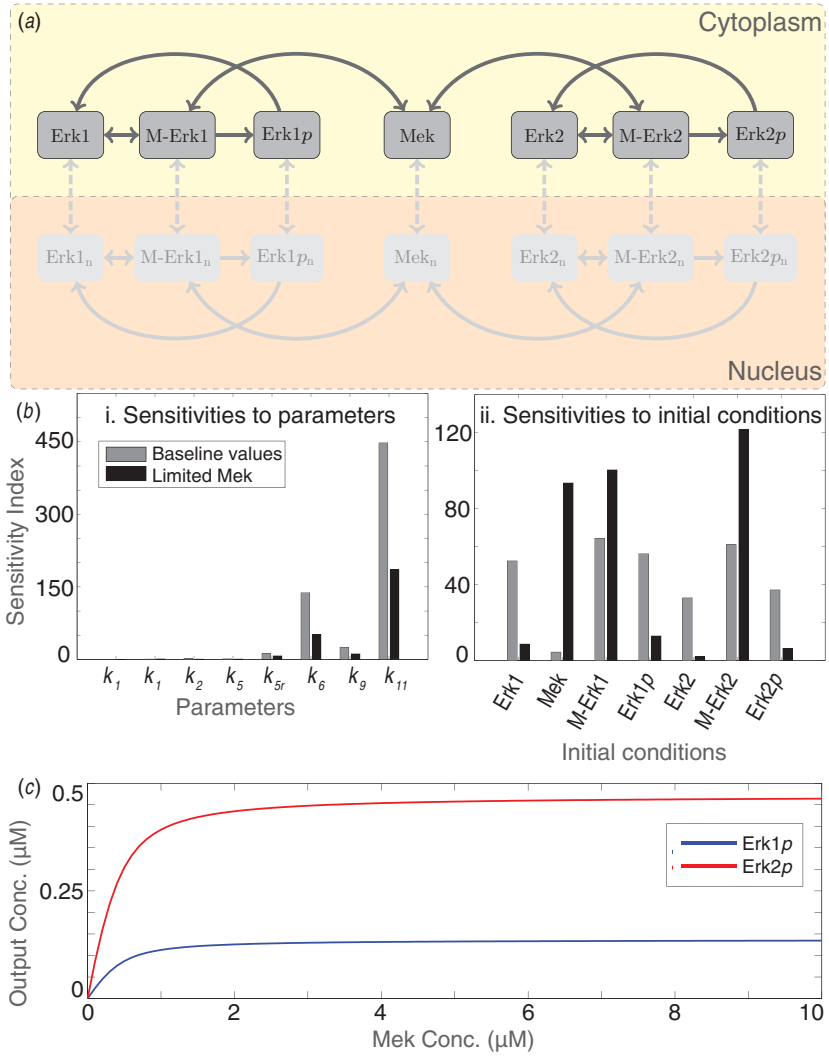

Figure 3. Minimal model. (*a*) Schematic of the biochemical Erk/Mek model. (*b*) Sensitivity analysis for the biochemical model. Mean sensitivity index given by the violet line (see 'Materials and methods'). (i) Sensitivity to parameters. (ii) Sensitivities to initial concentration.

cytoplasm in the absence of stimulation, and accumulates in the nucleus upon stimulation [16].

Assuming a constant stimulus, as is the case for our experimental set-up, we simulate our model until steady state. The time course of active nuclear Erk is given in figure 1(*a*), and total nuclear Erk1 and Erk2 abundances are shown in figure S1(a) in the supplementary material (available at stacks.iop.org/PhysBio/9/036001/mmedia). We vary the initial concentrations of Erk and Mek within the known constraints; activation of the system is determined by the initial condition of active Mek. Mek then activates Erk, which can then traffic into and out of the nucleus; we are therefore interested in both the transient *activation time* (time until a species reaches steady state) and the realized *steady-state* values of Erk1p_{n} and Erk2p_{n} (phospho-nuclear Erk1/2).

The overarching question is really why do nearly identical Erk1 and Erk2 proteins exist? In particular, we seek to address this question by considering two related questions in more detail: (1) How does the behavior of these variants differ in different cell types and under different physiological conditions? (2) How does nuclear shuttling differ between the two proteins, and how does this affect the overall nuclear activity levels of Erk? More generally, we develop a flexible mechanistic description of Erk-mediated signaling that includes the nuclear translocation dynamics. This framework can be adapted to other molecules, e.g., NFAT, Stat3/5 [52], etc, where we have distinct biochemical isoforms with different nuclear shuttling dynamics.

Minimal model

To address the above questions, the behavior of Erk isoforms under varying physical conditions is more closely studied in the absence of transport (figure 3(*a*)). Sensitivity analyses identify Erk1p and Erk2p concentrations as most sensitive to the phosphorylation/dephosphorylation (k_6, k_{11}) rates of Erk1 and Erk2 (figure 3(*b*)). The analysis of the initial conditions also shows that the available phosphorylated Mek increases in importance at lower signal strength (limited Mek) (figure 3(*b*)) and (*c*)), which in an experimental context is what we expect. The percentage of Mek that is usually phosphorylated depends on signal strength and this enzyme

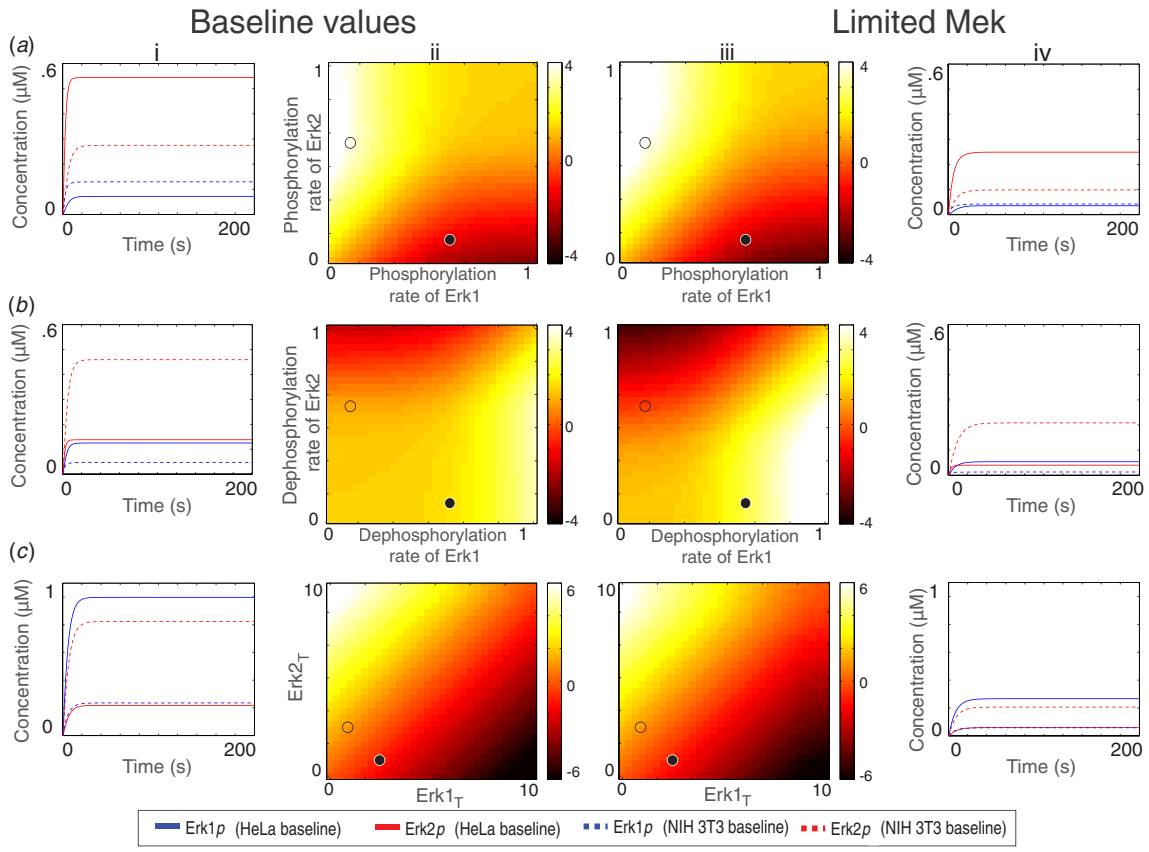

Figure 4. Competition in the minimal model at baseline and limited Mek (Mek=0.2) conditions. Heat maps (ii)–(iii) show the values of the ratio $\varphi = \log(\text{Erk2}p/\text{Erk1}p)$ (see the text) for different parameter/initial condition combinations. The ratios, φ, at the steady state ((i), (iv)) are indicated by solid/empty circles in the heat map and correspond to the solid/dotted lines in columns (i) and (iv). (*a*) Effects of phosphorylation rates on Erk1/2*p*. Values of (k_2, k_6) are varied; the solid circle (solid line) represents high $k_2 = 0.6$, low $k_6 = 0.1$, and the open circle (dotted line) represents low $k_2 = 0.1$, high $k_6 = 0.6$. (*b*) Effects of dephosphorylation rates on Erk1/2*p*. Values of (k_9, k_{10}) are varied; the solid circle (solid line) represents high $k_9 = 0.6$, low $k_{10} = 0.1$, and the open circle (dotted line) represents low $k_9 = 0.1$, high $k_{10} = 0.6$. (*c*) Effects of Erk1 and Erk2 initial conditions. Values of total Erk concentrations (Erk1_T, Erk2_T) are varied; the solid circle (solid line) represents high $\text{Erk1}_T = 2$, low $\text{Erk2}_T = 0.5$, and the open circle (dashed line) represents low $\text{Erk1}_T = 0.5$, high $\text{Erk2}_T = 2$.

would greatly affect the steady state of Erk*p*. The balance between phosphorylation/dephosphorylation rates and initial conditions provides a setting for a competition scheme between Erk isoforms for its activator Mek.

We are interested in the effects of the phosphorylation/dephosphorylation rates on the relative abundances of Erk2*p* to Erk1*p* at baseline Mek and limited Mek conditions. By defining a log-scale indicator

$$\varphi = \log\left(\frac{\text{Erk2}p}{\text{Erk1}p}\right),$$

the sign of φ signifies the dominance of a specific phospho-Erk isoform (a positive value denotes Erk2*p* > Erk1*p* and a negative value indicates Erk1*p* > Erk2*p*). The phosphorylation rates and dephosphorylation rates are each varied separately from 10^{-3} to 10^{1} in line with biophysical considerations, and φ is shown in figures 4(*a*) and (*b*). As the rate of Erk1 phosphorylation increases, φ becomes negative indicating the dominance of Erk1*p* (see the bottom-right corner of figure 4(*a*) (ii)), whereas an increase in Erk2 phosphorylation rate leads to Erk2 prevalence. The effect of the phosphorylation rate on φ is, however, asymmetric, with a larger region in parameter space giving rise to Erk2*p* dominance (see the non-overlapping curves in figure 4(*a*) (i)). Notably, the competition is exacerbated under limited Mek conditions where the maximum/minimum values of φ are larger and smaller, respectively, than the baseline conditions. Inspection of the dephosphorylation rates shows that an increase in the dephosphorylation rate of Erk1 results in a larger positive φ, or an Erk2*p* steady-state bias, and vice versa for Erk2 dephosphorylation. This is also reflected in the heat map representation which clearly shows this asymmetry, and the time course (figure 4(*b*) (i)), where equality between Erk1*p* and Erk2*p* steady-state values exists for slow dephosphorylation of Erk1, but not for slow Erk2 dephosphorylation (figure 4(*b*) (i)). Under *limited Mek* conditions, both Erk1*p* and Erk2*p* steady-state values are much reduced and activation time increases (figures 4(*a*) and (*b*) (iv)). For limited Mek conditions, the phosphorylation/dephosphorylation rate parameter space has a larger region allowing for competition scenarios (see the largest (white) and smallest (black) values of φ, corresponding to high Erk2*p* and Erk1*p* dominance in figures 4(*a*) and (*b*) (iii)). This suggests that for certain phosphorylation/dephosphorylation rates, a limited

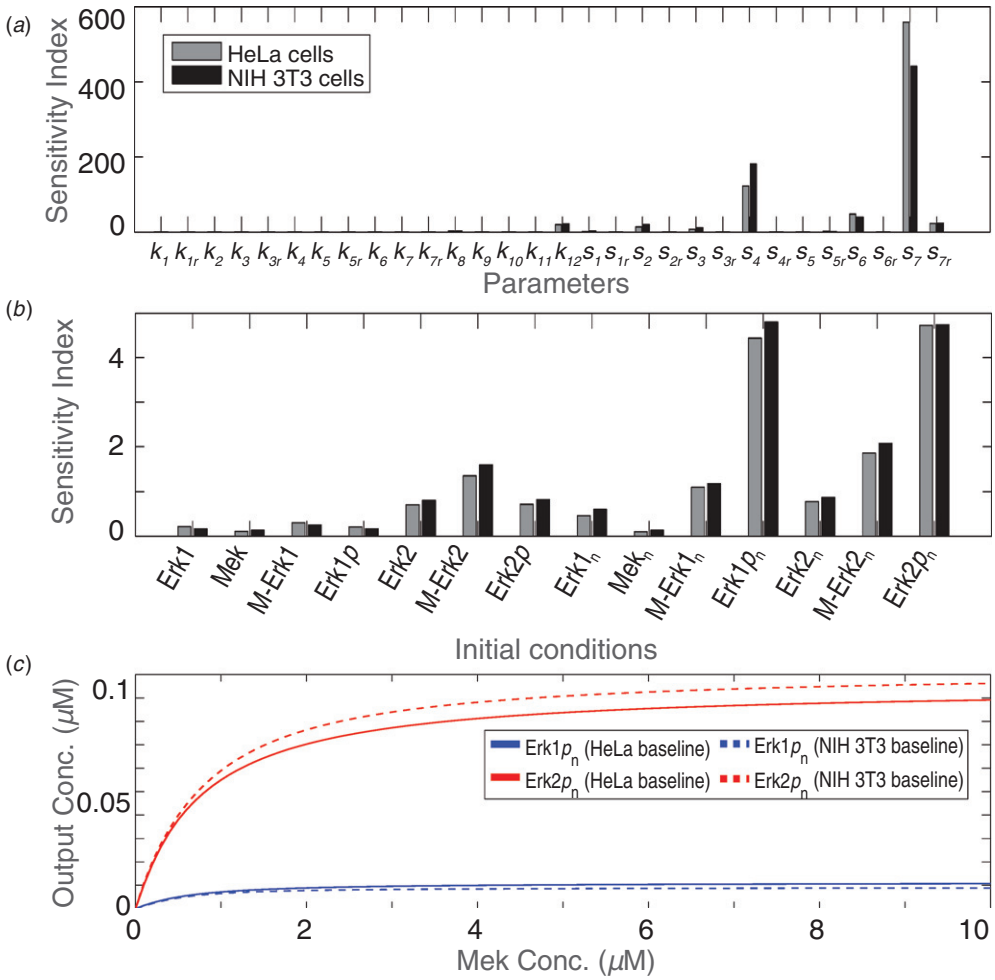

Figure 5. Sensitivity coefficients for parameters (*a*) and initial conditions (*b*). For both HeLa and NIH cells, only a limited number of parameters have a significant influence on the behavior of Erk1p_n and Erk2p_n: s_7, s_4, s_6, s_{7r}, k_{12}, s_2, s_3. Sensitivity to initial conditions reveals that for both cell types, all initial conditions have a comparable impact on the observed dynamics. The most sensitive initial conditions, however, are much less sensitive than most sensitive parameters. (*c*) Effects of phosphorylated Mek on output concentrations Erk1p_n and Erk2p_n.

stimulus would more strongly favor Erk1p. Unlike the phosphorylation/dephosphorylation cases, the value of φ at a given total (Erk1, Erk2) concentration does not change as Mek becomes limited (heat map indicator colors are nearly identical in figure 4(*c*)).

The minimal model offers a number of insights, specifically that phosphorylation/dephosphorylation rates play an important role in setting the steady-state behavior of Erk1p and Erk2p. Under limited Mek conditions, the parameter rate space suggests a stronger effect (larger $|\varphi|$) on the response. The value of the initial conditions can induce an Erk2p- or Erk1p-dominated response, and limiting Mek alters the steady-state value of this response.

Complete system

The minimal model provides preliminary insights into the behavior of Mek and Erk1/2. But further analysis of the complete system is required to elucidate the role of translocation between the two cellular compartments (cytoplasm and nucleus).

As shown in figure 5(*a*), the equilibration dynamics and steady state of Erk1p_n and Erk2p_n in HeLa and NIH 3T3 cells are most sensitive to the import shuttling rates of Erk1p, Erk2p and M-Erk2 (s_4, s_7, s_3), and the only sensitive biochemical reaction rate is the dephosphorylation rate of Erk2p_n (k_{12}). The primary difference between the cell types is the sensitivity to Erk protein shuttling speeds. Specifically, HeLa cells are more sensitive to Erk2p import shuttling, whereas NIH 3T3 cells are more responsive to changes in Erk1p. Overall, both cell types are quantitatively most sensitive to the shuttling of Erk2. This analysis also highlights the similarities and differences in sensitivity between initial conditions of the minimal model and the complete system (figure 5(*b*)). The intermediary complex of Mek–Erk2 is sensitive in both models and the nuclear complexes are also sensitive. The pronounced difference in steady-state concentrations between the two cell conditions (limited Mek and baseline) that was observed in the minimal model does not transpire in the complete model. As shown in figures 5(*a*) and (*b*), the sensitivity index of the most important parameters is nearly 100 times those of the initial conditions. Investigating the stimulus-response curve reveals

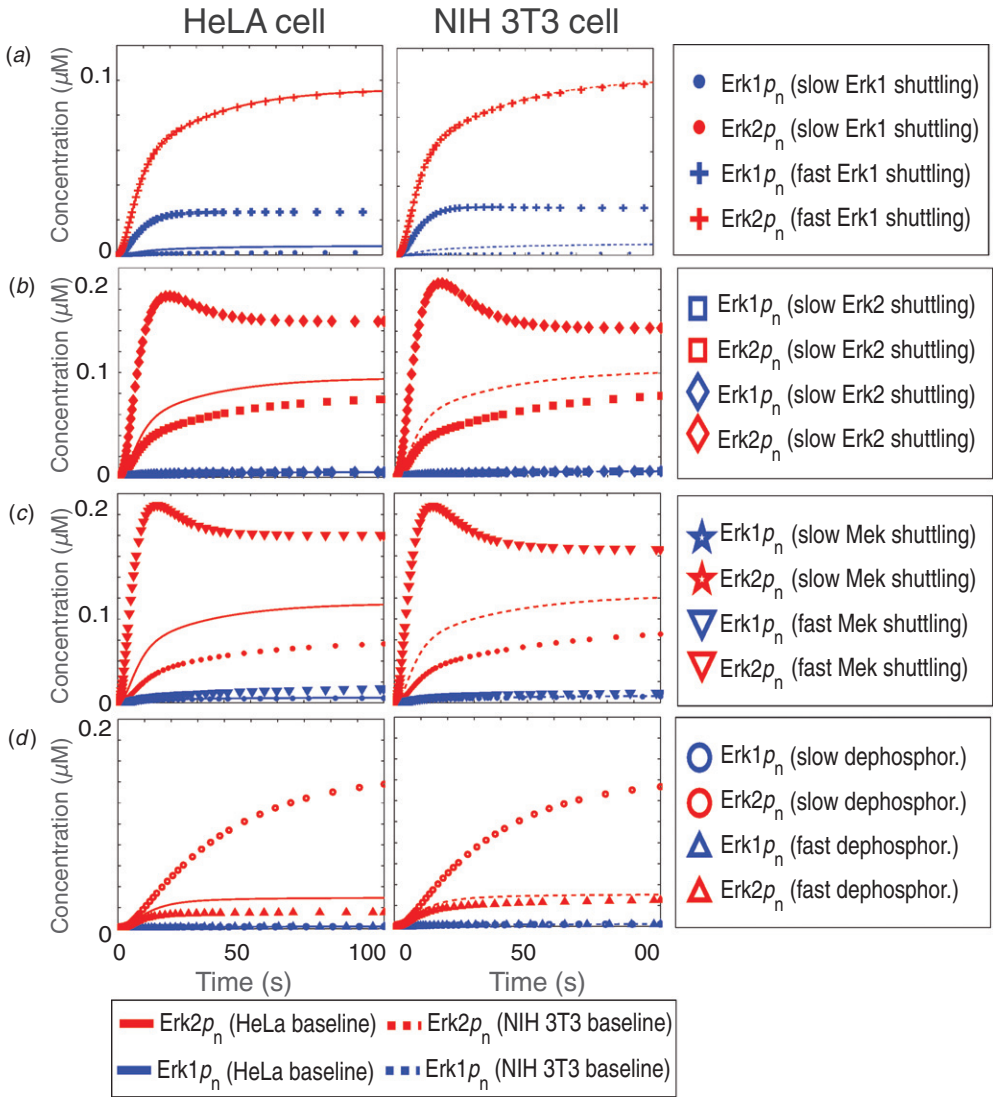

Figure 6. Effects of Erk and Mek shuttling, and dephosphorylation rates on complete model solution curves at baseline parameter values and initial conditions. The solid line denotes the HeLa cell baseline and the dotted line denotes the NIH 3T3 cell baseline. (*a*),(*b*) Effect of Erk1*p* (s_4) and Erk2*p* (s_7) shuttling rates. Parameters are varied by an order of magnitude from their baseline values. Erk1*p* shuttling: slow (dots) and fast (cross). Erk2*p* shuttling rates: slow (squares) and fast (diamonds). (*c*) Effects of Mek shuttling rates (s_2, s_3 and s_6): slow (stars), fast (upside-down diamonds). (*d*) Effects of dephosphorylation rate of Erk2*p* (k_{12}). Slow dephosphorylation ($k_{12} = 0.014$) is denoted by circles and fast rate ($k_{12} = 0.6$) is represented by triangles.

that unlike the minimal model, Mek(0) = 1 does not saturate Erk2p_n but requires a stronger stimulus (compare figures 3(*c*) and 5(*c*)). The sensitivity analysis was repeated for limited Mek conditions, which did not present any difference in the importance of parameters or initial conditions.

Given the importance of the shuttling rates on Erk1p_n and Erk2p_n concentrations, we further investigate the response of HeLa and NIH 3T3 cells to different factors affecting shuttling. For both cell types, we find that increasing the Erk1*p* shuttling rates (figure 6(*a*)), Erk2*p* shuttling rates (figure 6(*b*)) and Mek shuttling (figure 6(*c*)) by an order of magnitude naturally increases the steady state and the activation time. While the sensitivity analysis suggests that NIH 3T3 cells are more sensitive to Erk1*p* shuttling, the differences between figure 6(*a*) (i)–(ii) are slight. In NIH 3T3 cells, the activation time of Erk1p_n is shorter and the steady state is slightly elevated. As expected, varying shuttling parameters for Erk1, for example, only affects the steady-state value of Erk1p_n. As the shuttling parameters are varied, we note that Erk2p_n steady-state values exhibit quantitatively larger difference than Erk1p_n. This difference confirms why Erk2*p* shuttling is the most sensitive parameter.

Mek shuttling affects Erk2p_n more than Erk1p_n both in activation time and steady-state value (figure 6(*c*)). While it is well known that Mek has a nuclear exclusion sequence that exports it from the nucleus, studies have suggested that Mek may play an active role in the transport of Erk [53, 54]. Our findings that the shuttling of Mek is less sensitive than Erk1*p*/Erk2*p*, yet has the same effect on steady state and activation time (compare figures 6(*b*) and 6(*c*)), are somewhat counterintuitive. Evidence suggests that the Mek-mediated contribution to Erk export is at most marginal under physiological conditions, and only contributes to the steady state in unphosphorylated conditions [13]. This may be due

to the very low rate supported by the CRM1-mediated export. Thus, our analysis has the unexpected result that Mek shuttling sensitivity is relatively small compared to Erk1*p* and Erk2*p* shuttling sensitivities, whereas simulations predict that Mek and Erk shuttling should have the same effect on activated nuclear Erk.

The effects of dephosphorylation on phospho-nuclear Erk steady states is more pronounced than the effect of phosphorylation rates (figure 6(*d*)). By decreasing the dephosphorylation rate of Erk2 (k_{12}) by an order of magnitude, we observe an increase in the steady-state value of Erk2p_n; increasing the dephosphorylation rate (more than fourfold) decreases the steady state to approximately half of the baseline value. The potential for increasing the activation time and steady-state value of Erkp_n by changing the dephosphorylation rates is in line with the minimal model results; however, the phosphorylation rates do not exhibit a notable change in either activation or steady state of Erkp_n in the full model.

The complete system thus shows how the shuttling rates of phosphorylated Erk affect the steady-state values of Erk1p_n and Erk$p$2$_n$ (figure 5(*a*)). The sensitivity analysis for HeLa cells suggests that their dynamics are somewhat more sensitive to Erk2*p* shuttling, whereas NIH 3T3 cells are more sensitive to Erk1*p* shuttling; however, our simulations do not show pronounced differences between the two cell types. We also observe that both cell types are responsive to Mek shuttling speeds although Mek shuttling parameters are not overly sensitive in analysis, which may explain the ongoing investigations of the role of Mek shuttling on Erk.

Discussion

Our analysis suggests that transport and shuttling of Erk are crucial for determining activity levels, overriding the effects of phosphorylation and dephosphorylation in many instances under physiological conditions. Competition between Erk1 and Erk2 for Mek is induced as biochemical rates and total concentrations of Erk and Mek change.

The subtle differences between cell types are also illuminating: since the shuttling rates are the most sensitive parameter, one may be led to think that differences in trafficking are at the basis for heterogeneity. There are two additional points, however, that we feel are pertinent in this context: (1) the composition and amount of nucleoporins changes during the cell cycle, which bring about changes in trafficking rates and in levels of Erk activation; (2) in neuronal cells, where trafficking rates are maximally different between Erk1 and Erk2 (unpublished data), we may expect enhanced differences between Erk1 and Erk2 activation levels. This is notable (it is certainly enthralling from a neurobiological point of view) since the only clear reported phenotype of the Erk1 knockout is neurophysiological. Although beyond the scope of this study, considering transient changes in Erk concentration as well as exploring the effects of downstream substrates may pin down the physiological implication of the shuttling mechanisms discussed here.

In response to a given stimulus, the different activation times are mostly due not to differences in the phosphorylation–dephosphorylation rates, but to differences in shuttling speed. The FRAP experiments show that there is a large variability in trafficking speed, likely due to the variable density of nucleoporins, and this could go a long way toward justifying the different kinetics. In view of the large individual differences between cells, these seem to be interesting and hitherto neglected aspects of studies of cell-to-cell variability. The development of these abstractions and sensitivity analysis as performed might help to understand what are the most likely parameters responsible for the heterogeneous responses within a cell population.

More generally, our results highlight the important aspect of spatial localization of specific isoforms that has hitherto often been neglected in models and experiments. Similarly to MAPK studies, NFAT has been found to have different behavior based on stimuli duration (sustained, pulsed, etc); notably, NFAT isoforms in the calcium/NFAT pathway that regulate T cells have different timed responses which may be explained by tissue-specific subcellular localization (Nir Friedman, personal communications). These are not isolated cases; thus, we feel that differential shuttling of similar signaling molecules coupled to competition between them may have a more general role in cellular decision-making processes.

Acknowledgments

HAH and MPHS gratefully acknowledge funding from Leverhulme Trust. MBD is supported by a BBSRC-Microsoft Research Dorothy Hodgkin Postgraduate Award. MK acknowledges support from the Biotechnology and Biological Sciences Research Council (BBSRC) (BB/G020434/1). PRIN 2008 from MIUR to GMR.

References

[1] Muller M and Ram P T 2010 Systems biology of the MAPK1, 2 network *Syst. Biol. Signaling Netw.* **1** 455–89

[2] Reszka A A, Seger R, Diltz C D, Krebs E G and Fischer E H 1995 Association of mitogen-activated protein kinase with the microtubule cytoskeleton *Proc. Natl Acad. Sci. USA* **92** 8881–5

[3] Fukuda M, Gotoh Y and Nishida E 1997 Interaction of MAP kinase with MAP kinase kinase: its possible role in the control of nucleocytoplasmic transport of MAP kinase *EMBO J.* **16** 1901–8

[4] Casar B, Sanz-Moreno V, Yazicioglu M N, Rodríguez J, Berciano M T and Lafarga M *et al* 2007 Mxi2 promotes stimulus-independent ERK nuclear translocation *EMBO J.* **26** 635–46

[5] Matsubayashi Y, Fukuda M and Nishida E 2001 Evidence for existence of a nuclear pore complex-mediated, cytosol-independent pathway of nuclear translocation of ERK MAP kinase in permeabilized cells *J. Biol. Chem.* **276** 41755–60

[6] Whitehurst A W, Wilsbacher J L, You Y, Luby-Phelps K, Moore M S and Cobb M H 2002 ERK2 enters the nucleus by a carrier-independent mechanism *Proc. Natl Acad. Sci. USA* **99** 7496–501

[7] Chuderland D, Konson A and Seger R 2008 Identification and characterization of a general nuclear translocation signal in signaling proteins *Mol. Cell.* **31** 850–61

[8] Plotnikov A, Chuderland D, Karamansha Y, Livnah O and Seger R 2011 Nuclear extracellular signal-regulated kinase 1 and 2 translocation is mediated by casein kinase 2 and accelerated by autophosphorylation *Mol. Cell. Biol.* **31** 3515–30

[9] Zehorai E, Yao Z, Plotnikov A and Seger R 2010 The subcellular localization of MEK and ERK—a novel nuclear translocation signal (NTS) paves a way to the nucleus *Mol. Cell. Endocrinol.* **314** 213–20

[10] Pouysségur J, Volmat V and Lenormand P 2002 Fidelity and spatio-temporal control in MAP kinase (ERKs) signalling *Biochem. Pharmacol.* **64** 755–63

[11] Pouysségur J and Lenormand P 2003 Fidelity and spatio-temporal control in MAP kinase (ERKs) signalling *Eur. J. Biochem./FEBS.* **270** 3291–9

[12] Ando R, Mizuno H and Miyawaki A 2004 Regulated fast nucleocytoplasmic shuttling observed by reversible protein highlighting *Science* **306** 1370–3

[13] Costa M, Marchi M, Cardarelli F, Roy A, Beltram F and Maffei L *et al* 2006 Dynamic regulation of ERK2 nuclear translocation and mobility in living cells *J. Cell Sci.* **119** 4952–63

[14] Marchi M, Pancrazi L, Maffei M, Ratto G M and Costa M 2010 ERK1 nucleocytoplasmic shuttling rate depends on specific N-terminal aminoacids *Biochem. Biophys. Res. Commun.* **398** 166–72

[15] Volmat V, Camps M, Arkinstall S, Pouysségur J and Lenormand P 2001 The nucleus, a site for signal termination by sequestration and inactivation of p42/p44 MAP kinases *J. Cell. Sci.* **114** 3433–43 PMID: 11682603

[16] Marchi M, D'Antoni A, Formentini I, Parra R, Brambilla R and Ratto G M *et al* 2008 The N-terminal domain of ERK1 accounts for the functional differences with ERK2 *PLoS One* **3** e3873

[17] Mazzucchelli C, Vantaggiato C, Ciamei A, Fasano S, Pakhotin P and Krezel W *et al* 2002 Knockout of ERK1 MAP kinase enhances synaptic plasticity in the striatum and facilitates striatal-mediated learning and memory *Neuron* **34** 807–20

[18] Pagès G, Guérin S, Grall D, Bonino F, Smith A and Anjuere F *et al* 1999 Defective thymocyte maturation in p44 MAP kinase (Erk 1) knockout mice *Science* **286** 1374–7

[19] Lefloch R, Pouysségur J and Lenormand P 2008 Single and combined silencing of ERK1 and ERK2 reveals their positive contribution to growth signaling depending on their expression levels *Mol. Cell. Biol.* **28** 511–27

[20] Ferrell J 1996 Tripping the switch fantastic: how a protein kinase cascade can convert graded inputs into switch-like outputs *Trends Biochem. Sci.* **21** 460–6

[21] Ferrell J E and Bhatt R R 1997 Mechanistic studies of the dual phosphorylation of mitogen-activated protein kinase *J. Biol. Chem.* **272** 19008–16

[22] Huang C Y and Ferrell J 1996 Ultrasensitivity in the mitogen-activated protein kinase cascade *Proc. Natl Acad. Sci. USA* **93** 10078–83

[23] Xiong W and Ferrell J 2003 A positive-feedback-based bistable 'memory module' that governs a cell fate decision *Nature* **426** 460–5

[24] Ferrell J 1997 How responses get more switch-like as you move down a protein kinase cascade *Trends Biochem. Sci.* **22** 288–9

[25] Angeli D, Ferrell J and Sontag E D 2004 Detection of multistability, bifurcations, and hysteresis in a large class of biological positive-feedback systems *Proc. Natl Acad. Sci. USA* **101** 1822–7

[26] Markevich N I, Hoek J B and Kholodenko B N 2004 Signaling switches and bistability arising from multisite phosphorylation in protein kinase cascades *J. Cell. Biol.* **164** 353–9

[27] Legewie S, Schoeberl B, Blüthgen N and Herzel H 2007 Competing docking interactions can bring about bistability in the MAPK cascade *Biophys. J.* **93** 2279–88

[28] Kholodenko B N 2000 Negative feedback and ultrasensitivity can bring about oscillations in the mitogen-activated protein kinase cascades *Eur. J. Biochem./FEBS* **267** 1583–8

[29] Ventura A C, Sepulchre J A and Merajver S D 2008 A hidden feedback in signaling cascades is revealed *PLoS Comput. Biol.* **4** e1000041

[30] Qiao L, Nachbar R B, Kevrekidis I G and Shvartsman S Y 2007 Bistability and oscillations in the Huang–Ferrell model of MAPK signaling *PLoS Comput. Biol.* **3** 1819–26

[31] Radhakrishnan K, Edwards J, Lidke D, Jovin T, Wilson B and Oliver J 2009 Sensitivity analysis predicts that the ERK–pMEK interaction regulates ERK *Syst. Biol.* **3** 329–41

[32] Zumsande M and Gross T 2010 Bifurcations and chaos in the MAPK signaling cascade *J. Theor. Biol.* **265** 481–91

[33] Heinrich R, Neel B G and Rapoport T A 2002 Mathematical models of protein kinase signal transduction *Mol. Cell.* **9** 957–70

[34] Behar M, Hao N, Dohlman H G and Elston T C 2007 Mathematical and computational analysis of adaptation via feedback inhibition in signal transduction pathways *Biophys. J.* **93** 806–21

[35] Qu Z and Vondriska T M 2009 The effects of cascade length, kinetics and feedback loops on biological signal transduction dynamics in a simplified cascade model *Phys. Biol.* **6** 16007

[36] Schilling M, Maiwald T, Hengl S, Winter D, Kreutz C and Kolch W *et al* 2009 Theoretical and experimental analysis links isoform-specific ERK signalling to cell fate decisions *Mol. Syst. Biol.* **5** 334

[37] Fujioka A, Terai K, Itoh R E, Aoki K, Nakamura T and Kuroda S *et al* 2006 Dynamics of the Ras/ERK MAPK cascade as monitored by fluorescent probes *J. Biol. Chem.* **281** 8917–26 PMID: 16418172

[38] Shankaran H, Ippolito D L, Chrisler W B, Resat H, Bollinger N and Opresko L K *et al* 2009 Rapid and sustained nuclear-cytoplasmic ERK oscillations induced by epidermal growth factor *Mol. Syst. Biol.* **5** 332

[39] Kholodenko B N, Hancock J F and Kolch W 2010 Signalling ballet in space and time *Nature Rev. Mol. Cell. Biol.* **11** 414–26

[40] Kholodenko B N and Birtwistle M R 2009 Four-dimensional dynamics of MAPK information processing systems *Wiley Interdiscip. Rev. Syst. Biol. Med.* **1** 28–44

[41] Vantaggiato C, Formentini I, Bondanza A, Bonini C, Naldini L and Brambilla R 2006 ERK1 and ERK2 mitogen-activated protein kinases affect Ras-dependent cell signaling differentially *J. Biol.* **5** 14 PMID: 16805921

[42] Schoeberl B, Eichler-Jonsson C, Gilles E D and Muller G 2002 Computational modeling of the dynamics of the MAP kinase cascade activated by surface and internalized EGF receptors *Nature Biotechnol.* **20** 370–5

[43] McKay M, Beckman R and Conover W 1979 A comparison of three methods for selecting values of input variables in the analysis of output from a computer code *Technometrics* **21** 239–45

[44] Feliu E and Wiuf C 2011 Enzyme sharing as a cause of multistationarity in signaling systems *J. R. Soc. Interface* **9** 1224–32

[45] Rand D A 2008 Mapping global sensitivity of cellular network dynamics: sensitivity heat maps and a global summation law *J. R. Soc. Interface* **5** S59–69
[46] Zwillinger D 1998 *Handbook of Differential Equations* (New York: Academic)
[47] Kass R E 1989 The geometry of asymptotic inference *Stat. Sci.* **4** 188–219
[48] Lenormand P P, Sardet C C and Pouysségur J J 1993 Growth factors induce nuclear translocation of MAP kinases (p42mapk and p44mapk) but not of their activator MAP kinase kinase (p45mapkk) in fibroblasts *J. Cell. Biol.* **122** 1079–88
[49] Rubinfeld H H, Hanoch T T and Seger R R 1999 Identification of a cytoplasmic-retention sequence in ERK2 *J. Biol. Chem.* **274** 30349–52
[50] Caunt C J and McArdle C A 2010 Stimulus-induced uncoupling of extracellular signal-regulated kinase phosphorylation from nuclear localization is dependent on docking domain interactions *J. Cell. Sci.* **123** 4310–20 PMID: 21123621
[51] Caunt C J and McArdle C A 2012 ERK phosphorylation and nuclear accumulation: insights from single-cell imaging *Biochem. Soc. Trans.* **40** 224–9
[52] Timmer J, Muller T, Swameye I and Sandra O 2004 Modeling the nonlinear dynamics of cellular signal transduction *Int. J. Bifurcation Chaos* **14** 2069–79
[53] Adachi M, Fukuda M and Nishida E 2000 Nuclear export of MAP kinase (ERK) involves a MAP kinase kinase (MEK)-dependent active transport mechanism *J. Cell. Biol.* **148** 849–56
[54] Adachi M, Fukuda M and Nishida E 1999 Two co-existing mechanisms for nuclear import of MAP kinase: passive diffusion of a monomer and active transport of a dimer *EMBO J.* **18** 5347–58